Almost sharp fronts for the surface geostrophic equation

Roberta Graff [*], **Javier de Ruiz Garcia** [†], **and Franklin Sonnery** [†]

[*]University of Cambridge, Cambridge, United Kingdom, and [†]Universidad de Murcia, Bioquimica y Biologia Molecular, Murcia, Spain

Submitted to Proceedings of the National Academy of Sciences of the United States of America

We use heat kernels or eigenfunctions of the Laplacian to construct local coordinates on large classes of Euclidean domains and Riemannian manifolds (not necessarily smooth, e.g. with C^α metric). These coordinates are bi-Lipschitz on large neighborhoods of the domain or manifold, with constants controlling the distortion and the size of the neighborhoods that depend only on natural geometric properties of the domain or manifold. The proof of these results relies on novel estimates, from above and below, for the heat kernel and its gradient, as well as for the eigenfunctions of the Laplacian and their gradient, that hold in the non-smooth category, and are stable with respect to perturbations within this category. Finally, these coordinate systems are intrinsic and efficiently computable, and are of value in applications.

monolayer | structure | x-ray reflectivity | molecular electronics

Abbreviations: SAM, self-assembled monolayer; OTS, octadecyltrichlorosilane

In this article we study the evolution of "almost-sharp" fronts for the surface quasi-geostrophic equation. This 2-D active scalar equation reads for the surface quasi-geostrophic equation.

$$\frac{D\theta}{Dt} = \frac{\partial\theta}{\partial t} + u\cdot\nabla\theta = 0 \qquad [1]$$

where,

$$u = (u_1, u_2) = (-\frac{\partial\psi}{\partial y}, \frac{\partial\psi}{\partial x}) \qquad [2]$$

and,

$$(-\triangle)^{\frac{1}{2}}\psi = \theta\,, \qquad [3]$$

For simplicity we are considering fronts on the cylinder, i.e. we take (x, y) in $\mathbb{R}/_{\mathbb{Z}} \times \mathbb{R}$. In this setting we define $-\triangle^{-\frac{1}{2}}$ that comes from inverting the third equation by convolution with the kernel. To avoid irrelevant considerations at ∞ we will take η to be compactly supported

$$\frac{\chi(u,v)}{(u^2+v^2)^{\frac{1}{2}}} + \eta(u,v)$$

where $\chi(x,y)\,\epsilon\, C_0^\infty$, $\chi(x,y) = 1$ in $|x-y| \le r$ and $supp\chi$ is contained in $\{|x-y| \le R\}$ with $0 < r < R < \frac{1}{2}$. Also $\eta\,\epsilon\, C_0^\infty$, $\eta(0,0) = 0$.

The main mathematical interest in the quasi-geostrophic equation lies in its strong similarities with the 3-Euler equations. These results were first proved by Constantin, Majda and Tabak, see [10], [11] and [12] for more details. There are several other research lines for this equation, both theoretical and numerical. See [13], [14], and [15]. The question about the regularity of the solutions for QG remains as an open problem.

Recently one of the authors has obtained the equation for the evolution of sharp fronts (in the periodic setting), proving its local well-posedness for that equation. (see [17] and [16] for more details). This is a problem in contour dynamics. Contour dynamics for other fluid equations has been studied extensively.

Analysis of almost sharp fronts

We begin our analysis on almost sharp fronts for the quasi-geostrophic equation recalling the notion of weak solution.

For these solutions we have the following

Definition 1. *A bounded function θ is a weak solution of QG if for any $\phi\,\epsilon\, C_0^\infty(\mathbb{R}/_{\mathbb{Z}} \times \mathbb{R} \times [0,\varepsilon])$ we have*

$$\int_{\mathbb{R}^+\times\mathbb{R}/_{\mathbb{Z}}\times\mathbb{R}} \theta(x,y,t)\,\partial_t\phi\,(x,y,t)dydxdt + \\ + \int_{\mathbb{R}^+\times\mathbb{R}/_{\mathbb{Z}}\times\mathbb{R}} \theta\,(x,y,t)u(x,y,t)\cdot\nabla\phi\,(x,y,t)dydxdt = 0 \quad [4]$$

where u is determined by equations **[2]** *and* **[3]**.

Data Sources. We are interested in studying the evolution of almost sharp fronts for the QG equation. These are weak solutions of the equation with large gradient ($\sim {}^1/_\delta$, where 2δ is the thickness of the transition layer for θ).

Discussion

Cylindrical Case. We are going to consider the cylindrical case here. We consider a transition layer of thickness smaller than 2δ in which θ changes from 0 to 1. (see Figure 1).That means we are considering θ of the form

$$\theta = 1 \text{ if } \quad y \ge \varphi(x,t) + \delta$$

$$\theta \text{ bounded if } \quad |\varphi(x,t) - y| \le \delta$$

$$\theta = 0 \text{ if } \quad y \le \varphi(x,t) - \delta \qquad [5]$$

where φ is a smooth periodic function and $0 < \delta < \frac{1}{2}$.

Significance

RJSM and ACAC developed the concept of the study. RJSM conducted the analysis, data interpretation and drafted the manuscript. AGB contributed to the development of the statistical methods, data interpretation and drafting of the manuscript.

Reserved for Publication Footnotes

Theorem 1. *If the active scalar θ is as in* [**5**] *and satisfies the equation* [**4**]*, then φ satisfies the equation*

$$\begin{aligned}\frac{\partial\varphi}{\partial t}(x,t) &= \int_{\mathbb{R}/\mathbb{Z}} \frac{\frac{\partial\varphi}{\partial x}(x,t)-\frac{\partial\varphi}{\partial u}(u,t)}{\left[(x-u)^2+(\varphi(x,t)-\varphi(u,t))^2\right]^{\frac{1}{2}}} \\ &\quad \chi(x-u,\varphi(x,t)-\varphi(u,t))du \;+ \\ &+ \int_{\mathbb{R}/\mathbb{Z}} \Big[\frac{\partial\varphi}{\partial x}(x,t)-\frac{\partial\varphi}{\partial u}(u,t)\Big] \\ &\quad \eta(x-u,\varphi(x,t)-\varphi(u,t))du + Error \quad [\mathbf{6}]\end{aligned}$$

with $|Error| \le C\,\delta|log\delta|$ where C depends only on $\|\theta\|_{L^\infty}$ and $\|\nabla\varphi\|_{L^\infty}$.

Remark 1. *Note that equation* [**5**] *specifies the function φ up to an error of order δ. Theorem 1 provides an evolution equation for the function φ up to an error of order $\delta|log\delta|$.*

In order to analyze the evolution of the "almost-sharp" front we substitute the above expression for θ in the definition of a weak solution (see [**4**]). We use the notation $X = O(Y)$ to indicate that $|X| \le C|Y|$ where the constant C depends only on $\|\theta\|_{L^\infty}$, $\|\nabla\varphi\|_{L^\infty}$ and $\|\phi\|_{C^1}$, where ϕ is a test function appearing in Definition 1.

We consider the 3 different regions defined by the form on θ. Since $\theta = 0$ in the region I the contribution from that region is 0, i.e.

$$\int_{I\times\mathbb{R}} \theta(x,y,t)\,\partial_t\phi\,(x,y,t)dydxdt+$$

$$+\int_{I\times\mathbb{R}} \theta\,(x,y,t)u(x,y,t)\cdot\nabla\phi\,(x,y,t)dydxdt = 0$$

As for the region II

$$\int_{II\times\mathbb{R}} \theta(x,y,t)\partial_t\phi(x,y,t)dxdydt = O(\delta)$$

since θ is bounded and hence $O(1)$, and the area of the region II is $O(\delta)$. As for the second term

$$\int_{II\times\mathbb{R}} u\theta\nabla\phi dxdydt = O(\delta log(\delta))$$

To see this, we fix t. We must estimate

$$\int_{\mathbb{R}^2} u\cdot(\not\Vdash_{II}\theta\nabla\phi)dxdy$$

We are left to estimate the terms

$$\int_{III\times\mathbb{R}} \theta\partial_t\phi dxdydt + \int_{III\times\mathbb{R}} \theta u_f\cdot\nabla\phi dxdydt =: A+B$$

Observations. The following observations can be made form the numerical experiments described in this section, and are consistent with the results of more extensive experimentation performed by the authors:

- The CPU times in Tables 1–3 are compatible with the estimates in formulae **14**, **16**, and **23**.
- The precision produced by each of Algorithms **I** and **II** is similar to that provided by formula **3**, even when ω_{k+1} is close to the machine precision.

Materials and Methods

Digital RNA SNP Analysis. A real-time PCR assay was designed to amplify **PLAC4** mRNA, with the two SNP alleles being discriminated by TaqMan probes. **PLAC4** mRNA concentrations were quantified in extracted RNA samples followed by dilutions to approximately one target template molecule of either type (i.e., either allele) per well. Details are given in the **SI Materials and Methods**.

Digital RCD Analysis. Extracted DNA was quantified by spectrophotometry (NanoDrop Technologies, Wilmington, DE) and diluted to a concentration of approximately one target template from either chr21 or ch1 per well.

Appendix: Estimating the Spectral Norm of a Matrix

In this appendix we describe a method for the estimation of the spectral norm of matrix A. The method does not require access to the individual entries of A; it requires only applications of A and A^* to vectors. It is a version of the classical power method. Its probabilistic analysis summarized below was introduced fairly recently in refs. 13 and 14. This appendix is included here for completeness.

Appendix

This is an example of an appendix without a title.

ACKNOWLEDGMENTS. This work was partially supported by Spanish Ministry of Science and Technology Grant BFM2002-02042 (to D.C. and J.L.R.) and by National Science Foundation Grand DMS-0245242 (to C.F.).

1. M. Belkin and P. Niyogi, Using manifold structure for partially labelled classification, Advances in NIPS, 15 (2003).
2. P. Bérard, G. Besson, and S. Gallot, Embedding Riemannian manifolds by their heat kernel, Geom. and Fun. Anal., 4 (1994), pp. 374–398.
3. R.R. Coifman and S. Lafon, Diffusion maps, Appl. Comp. Harm. Anal., 21 (2006), pp. 5–30.
4. R.R. Coifman, S. Lafon, A. Lee, M. Maggioni, B. Nadler, F. Warner, and S. Zucker, Geometric diffusions as a tool for harmonic analysis and structure definition of data. Part I: Diffusion maps, Proc. of Nat. Acad. Sci., (2005), pp. 7426–7431.
5. P. Das, M. Moll, H. Stamati, L. Kavraki, and C. Clementi, Low-dimensional, free-energy landscapes of protein-folding reactions by nonlinear dimensionality reduction, P.N.A.S., 103 (2006), pp. 9885–9890.
6. D. Donoho and C. Grimes, Hessian eigenmaps: new locally linear embedding techniques for high-dimensional data, Proceedings of the National Academy of Sciences, 100 (2003), pp. 5591–5596.
7. D. L. Donoho and C. Grimes, When does isomap recover natural parameterization of families of articulated images?, Tech. Report Tech. Rep. 2002-27, Department of Statistics, Stanford University, August 2002.
8. M. Grüter and K.-O. Widman, The Green function for uniformly elliptic equations, Man. Math., 37 (1982), pp. 303–342.
9. R. Hempel, L. Seco, and B. Simon, The essential spectrum of neumann laplacians on some bounded singular domains, 1991.
10. Kadison, R. V. and Singer, I. M. (1959) Extensions of pure states, Amer. J. Math. 81, 383-400.
11. Anderson, J. (1981) A conjecture concerning the pure states of $B(H)$ and a related theorem. in Topics in Modern Operator Theory, Birkhaüser, pp. 27-43.
12. Anderson, J. (1979) Extreme points in sets of positive linear maps on $B(H)$. J. Funct. Anal. 31, 195-217.
13. Anderson, J. (1979) Pathology in the Calkin algebra. J. Operator Theory 2, 159-167.
14. Johnson, B. E. and Parrott, S. K. (1972) Operators commuting with a von Neumann algebra modulo the set of compact operators. J. Funct. Anal. 11, 39-61.
15. Akemann, C. and Weaver, N. (2004) Consistency of a counterexample to Naimark's problem. Proc. Nat. Acad. Sci. USA 101, 7522-7525.
16. J. Tenenbaum, V. de Silva, and J. Langford, A global geometric framework for nonlinear dimensionality reduction, Science, 290 (2000), pp. 2319–2323.
17. Z. Zhang and H. Zha, Principal manifolds and nonlinear dimension reduction via local tangent space alignement, Tech. Report CSE-02-019, Department of computer science and engineering, Pennsylvania State University, 2002.

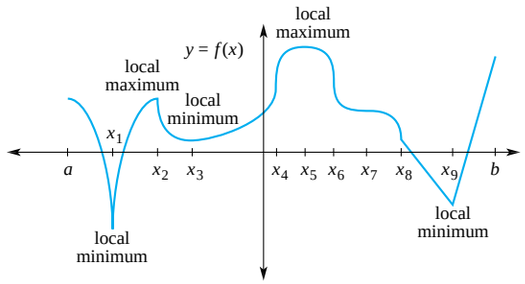

Fig. 1. LKB1 phosphorylates Thr-172 of AMPKα *in vitro* and activates its kinase activity.

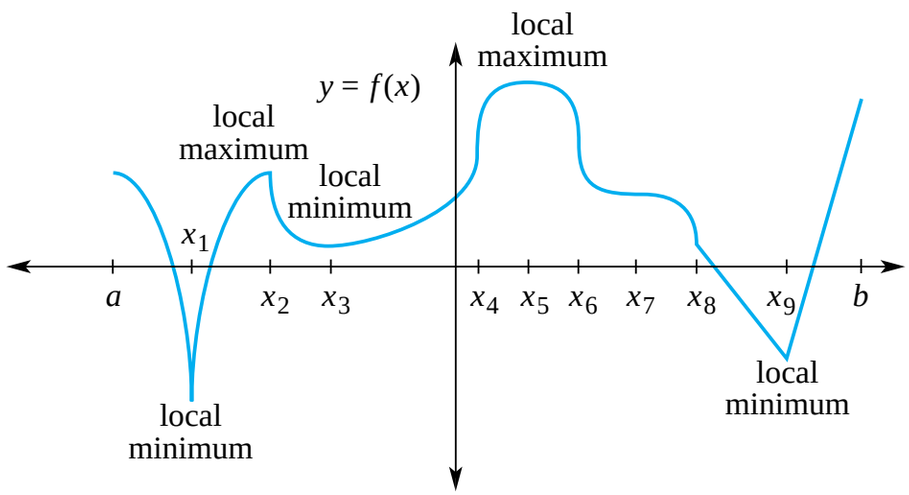

Fig. 2. LKB1 phosphorylates Thr-172 of AMPKα *in vitro* and activates its kinase activity.

Table 1. Repeat length of longer allele by age of onset class. This is what happens when the text continues.

Age of onset,	Repeat length				
years	n	Mean	SD	Range	Median
Juvenile, 2−20	40	60.15	9.32	43−86	60
Typical, 21−50	377	45.72	2.97	40−58	45
Late, >50	26	41.85	1.56	40−45	42*

*The no. of wells for all samples was 384. Genotypes were determined by mass spectrometric assay. The m_t value indicates the average number of wells positive for the over represented allele.

Table 2. Summary of the experimental results

Parameters		Averaged Results							Comparisons			
n	S^*_{MAX}	t_1	r_1	m_1	t_2	r_2	m_2	t_{lb}	t_1/t_2	r_1/r_2	m_1/m_2	t_1/t_{lb}
10*	1	4	.0007	4	4	.0020	4	4	1.000	.333	1.000	1.000
10†	5	50	.0008	8	50	.0020	12	49	.999	.417	.698	1.020
100‡	20	2840975	.0423	95	2871117	.1083	521	—	.990	.390	.182	—

*Stanford Synchrotron Radiation Laboratory (Stanford University, Stanford, CA)

†$R_{\mathrm{FREE}} = R$ factor for the $\sim 5\%$ of the randomly chosen unique reflections not used in the refinement.

‡Calculated for all observed data